Letter
Vol. 46, No. 15 / 1 August 2021 / Optics Letters 3769

Optics Letters

Narrow-linewidth single-polarization fiber laser using non-polarization optics

LIYUN HAO,[1] XIAOHAN WANG,[1] KUNPENG JIA,[1,2] GANG ZHAO,[1,3] ZHENDA XIE,[1,4] AND SHINING ZHU[1]

[1]National Laboratory of Solid State Microstructures, School of Electronic Science and Engineering, College of Engineering and Applied Sciences, and School of Physics, Nanjing University, Nanjing 210093, China
[2]e-mail: njujkp@gmail.com
[3]e-mail: zhaogang@nju.edu.cn
[4]e-mail: xiezhenda@nju.edu.cn

Received 21 June 2021; revised 6 July 2021; accepted 6 July 2021; posted 7 July 2021 (Doc. ID 434307); published 29 July 2021

Single longitudinal mode and single polarization are basic requirements of high performance fiber lasers, while their realizations are nontrivial, owing to the long laser cavity and lack of polarization selection of ordinary optical fibers. Here, we demonstrate an all-fiber narrow-linewidth laser realized on an external high-Q fiber ring, with combined functions of single-longitude-mode selection and linewidth reduction. A single-longitude-mode laser with a high polarization extinction ratio of ∼40 dB and low white frequency noise at 0.3 Hz^2/Hz is achieved, corresponding to a fundamental linewidth of ∼0.92 Hz. Using all non-polarization fiber components and ordinary gain fiber, our scheme shows the realization of narrow-linewidth single-polarization fiber lasers in a simple and cost-effective way, promising for broadband applications.

https://doi.org/10.1364/OL.434307

Narrow-linewidth fiber lasers feature easy fiber integration, high beam quality, and good frequency stability, and are attractive in various advanced laser applications [1,2]. For example, in coherent wind LIDAR, linewidth reduced fiber lasers are beneficial for the detection of small-Doppler-shift signals, corresponding to low wind speed [3]. Based on the instinctive narrow linewidth, a distributed feedback fiber laser active locking to a stabilized frequency reference can make a sub-10-mHz linewidth, satisfying the requirements of most atom clocks [4,5]. Further improving the linewidth can also bring advantages in high capacity communications with more wavelength division multiplexed fiber links to data center networks, which play important roles in our daily lives [6–8].

Single longitudinal mode and single polarization are basic requirements of high performance fiber lasers. However, owing to the long laser cavity, fiber lasers are usually in multi longitude mode lasing. Also, ordinary gain fibers are non-polarization selecting. The realization of single longitudinal mode and single polarization is not trivial in fiber lasers, with mechanisms such as very narrow filters [9,10], special fibers [11,12], and discrete polarizers required [13], and being expensive, sophisticated, or difficult in optical path stability.

Self-injection locking can efficiently reduce the linewidth of an exciting laser, without any locking circuits. In recent years, self-injection locking of fiber lasers has focused mainly on single-longitudinal-mode fiber lasers with long external fibers, where the linewidth-reduction efficiency relies on the length of the external fiber [12,14]. However, a too long external fiber inevitably couples more environmental noise, and is even worse with extra frequency sidebands [12]. In comparison, self-injection locking with an external high finesse resonator is an optimization over the external-cavity laser, with weak feedback, low environmental sensitivity, and substantial linewidth reduction [15,16], but is seldom reported in longitudinal mode selection.

In this Letter, we report on a fiber laser self-injection locked to an external high finesse fiber ring (fiber-R), with combined functions of single-longitudinal-mode selection and linewidth narrowing. Fiber-R is made with two ordinary fiber couplers, and reaches a high Q of 1.42×10^8, which is comparable to that of a finely fabricated spiral resonator at the same scale of length [17,18]. The laser system is truly all-fiber integrated, with fiber ends spliced for connecting. Single mode lasing with output power of 60 mW, high polarization extinction ratio (PER) of ∼40 dB, and very low white frequency noise at 0.3 Hz^2/Hz is measured, corresponding to a fundamental linewidth of ∼0.94 Hz. The high PER reached here comes from orthogonal polarized eigenmodes of the birefringent fiber laser [19] and efficient external longitudinal mode selection. With ordinary gain fiber and without any polarized elements, our scheme shows the realization of narrow-linewidth single-polarization fiber lasers in a simple and cost-effective way, promising for broadband applications.

Formation of fiber-R is shown in Fig. 1(a). It is composed of two 1/99 fused couplers (C2 and C3), with 1% input ends and 1% output ends spliced to form a closed loop, and has a round-trip length of ∼1.61 m. The couplers are made with SMF-28 fiber and have very low loss in tapers. A sweeping laser centered at 1550 nm together with an unbalanced fiber Mach–Zehnder interferometer (MZI) is used to characterize fiber-R. The MZI has a fiber difference of 23.5 m, and the corresponding sinusoidal curve measured at the same scanning is used to

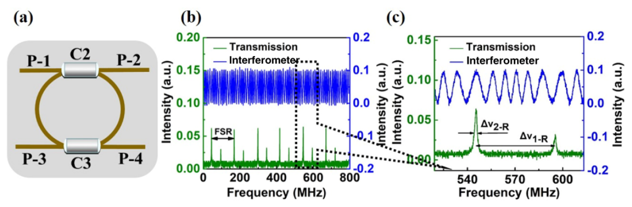

Fig. 1. Fiber-R and its characterization. (a) Schematic picture of fiber-R. C2 and C3 are 1/99 fused couplers made with SMF-28 fiber. P-1/P-2, P-3/P-4 are 99% input/output ports of C2, C3, respectively. (b) Olive curve: transmission signal when scanning a sweeping laser across resonance of fiber-R, FSR of 125 MHz. Blue curve: sinusoidal curve from the MZI at the same scanning for calibration. (c) Zoom-in of the two orthogonal polarized modes of fiber-R, with frequency separation of $\Delta\nu_{1-R} = 49$ MHz and resonance width of $\Delta\nu_{2-R} = 1.36$ MHz.

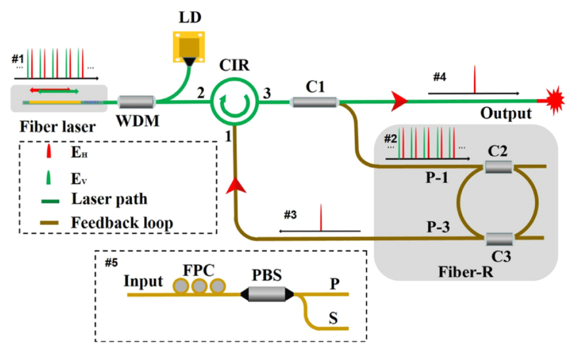

Fig. 2. Experimental setup. Fiber laser, birefringent fiber laser with multi longitudinal modes; E_H, E_V, electrical fields of longitudinal modes in two orthogonal polarizations; WDM, wavelength division multiplexing; LD, 980-nm laser diode; CIR, optical circulator; C1, 10/90 fiber coupler. Insets 1–4: evolutions of the longitudinal modes in the original fiber laser, before fiber-R, back injection, and output (E_H, for example), respectively. Inset 5: FPC-PBS setup used in the measurement. FPC, three-paddle fiber polarization controller; PBS, fiber polarization beam splitter.

calibrate frequency variations of the sweeping laser. With P-1 as the input and P-3 as the output to a photodetector (PD), transmission signals (olive curve) when scanning a sweeping laser across the resonance of fiber-R and the calibrating curve (blue curve) are shown in Figs. 1(b) and 1(c). Fiber-R has a free spectral range (FSR) of 125 MHz and resonance width of $\Delta\nu_{2-R} = 1.36$ MHz, corresponding to a finesse of 92 and Q factor of 1.42×10^8. Resonance peaks in different sets of intensities correspond to two orthogonally polarized modes of fiber-R, with a frequency separation of $\Delta\nu_{1-R} = 49$ MHz. Transmission efficiency of fiber-R is 31%, measured from the peak of the resonance to the input intensity.

Our experimental setup is schematically shown in Fig. 2. The fiber laser is constructed with a dielectric mirror (coated on the end of a well-polished Hi-1060 fiber with reflection of >99.6% around 1550 nm), a fiber Bragg grating (FBG, 3-dB bandwidth of 0.5 nm and reflection of 50% at 1549.8 nm), spliced on two ends of a 35-cm-long gain fiber (LIEKKI, Er80-8/125), with a total cavity length of ∼48 cm. It is back pumped by a 980-nm laser diode through a 980/1550-nm wavelength division multiplexer (WDM), and laser emission couples through the FBG and output from the signal port of the WDM. The laser diode (LD) is temperature controlled at 25°C with an accuracy of 0.01°C. The fiber laser is connected to port 2 of a three-port circulator (CIR), and light from port 3 of the CIR is directed to a 10/90 coupler to divide into two parts, where 90% of the total power serves as the output of the laser system. The remaining 10% is sent to fiber-R, with P-1 as the input port and P-3 as the output port connected to port 1 of the CIR to form the feedback loop. All the unillustrated fibers in the optical path are standing SMF-28 fiber, with fiber ends spliced together. The whole optical path is pressed on the optical platform with adhesive tape, for thermal cooling and vibrational stability. The operating principle of the longitudinal-mode-selection scheme is illustrated in the insets of Fig. 2 (1–4) showing the evolutions of the longitudinal modes in the original fiber laser, before fiber-R, back injection, and output respectively. In design, the fiber laser and the external fiber-R have mismatched FSRs. Fiber-R here works as an external bandpass filter to the longitudinal modes of the fiber laser. The only longitudinal mode on resonance of fiber-R is transmitted and injects back to the laser cavity, making its priority in the mode competition with other eigenmodes of the fiber laser suppressed. Single longitudinal mode occurs, with substantial linewidth reduction reached simultaneously from the self-injection-locking scheme.

The original performance of the fiber laser is measured at the output port of the WDM. Using a power meter, laser power versus the current of LD is shown in Fig. 3(a). The fiber laser has a maximum output power of 81 mW, at a pumping current of 700 mA. Longitudinal modes of the fiber laser are analyzed by directing the laser power to a fast PD (EOT, ET-5000 F) and fed into the electrical spectral analyzer (ESA, KEYSIGHT, N9020A). The radio frequency (RF) spectra acquired are shown in the blue curve in Fig. 3(b). The multi beat notes displayed confirm the multi-longitudinal-mode working of the fiber laser. Their frequency spacing of $\Delta\nu_H = 216$ MHz agrees well with the FSR calculated from the cavity length of the fiber laser. Orthogonally polarized eigenmodes of the fiber laser, owing to birefringence, are characterized by directing the laser power to a fiber polarization beam splitter, with a fiber polarization controller connected ahead [FPC-PBS setup, as shown in Fig. 2 (5)] to adjust their intensity in the P/S port of the PBS. The PBS is used to mix the orthogonally polarized longitudinal modes. The mixed RF spectra measured at the S-port of the PBS is shown in the black curve in Fig. 3(b). The added beat notes, in respect to the blue curve, come from frequency mixing of the orthogonally polarized longitudinal modes, with a frequency spacing of $\Delta\nu_{HV} = 43.5$ MHz. These longitudinal modes (influenced by other factors such as mode competition in the original laser and dispersion), with mismatched FSRs from fiber-R, finally result in single-longitudinal-mode transmission of the external fiber-R in the experiment. Power of the longitudinal modes in two polarization states is measured through the same FPC-PBS setup, with the FPC to adjust the maximum difference of the power at the P/S-port. The powers monitored are shown in Fig. 3(c), and their nearly same values indicate equivalent powers of the longitudinal modes in two orthogonal polarizations.

Single longitude mode of the injection-locked fiber laser is confirmed by only one beat note in the RF spectra of delayed self-heterodyne interferometry (DSHI) measurement. The DSHI setup is based on an unbalanced fiber MZI, with

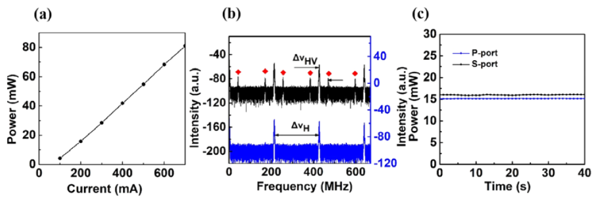

Fig. 3. Original performance of the fiber laser. (a) Power of the fiber laser verse current of the LD. (b) Longitudinal mode characterization. Blue curve: beat notes between longitudinal modes of the same polarization, $\Delta\nu_H = 216$ MHz. Black curve: added beat notes, with red ♦ above marked, come from mixing of the two orthogonal polarized longitudinal modes at S-port of the PBS, $\Delta\nu_{HV} = 43.5$ MHz. (c) Power characterization of the longitudinal modes in two polarizations.

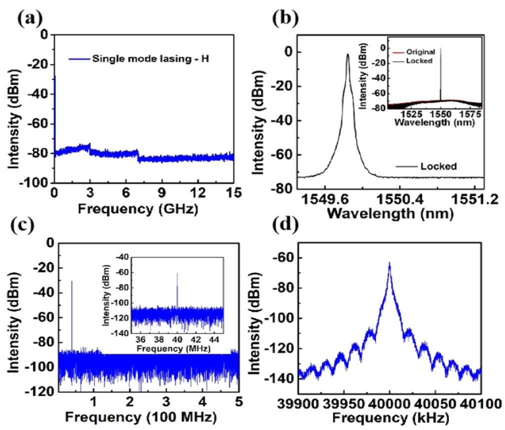

Fig. 4. Single longitudinal mode of the injection-locked fiber laser. (a) RF spectra from the DSHI measurement. (b) Optical spectrum measured by an OSA, with 3-dB width of 0.0179 nm and signal-to-noise ratio of >70 dB. Inset: broad spectrum of the locked laser (black curve) and original laser (red curve) for comparison. (c), (d) Zoom-in of the beat note around 40 MHz, in frequency span of 500 MHz (inset: 10 MHz) and 200 kHz.

~13244−m fiber delay on one arm and a 40-MHz acousto-optic modulator for frequency shifting on the other. A fast PD and an ESA are used to detect and analyze the beat signal from the MZI. In the experiment, the pumping current of the fiber laser is first set at a max of 700 mA, and then slightly tuned down to up-shift the frequency of the longitudinal modes in the fiber laser to make one on resonance of fiber-R. The current is given by an ordinary constant-current supply (THORLABS, LDC 240C, with resolution of 100 µA and accuracy of ±4.0 mA) without any feedback circuits. Single mode lasing is observed, with only one beat note at 40 MHz in a frequency span of 0–15 GHz, as shown in Fig. 4(a). Figure 4(b) is the optical spectrum measured at the same time using an optical spectrum analyzer (OSA), showing a 3-dB bandwidth of 0.0179 nm (corresponding to 2.23 GHz, which is within the 0.02-nm resolution limit of the OSA) and a signal-to-noise ratio of >70 dB. The measured optical spectrum further confirms that no other frequency modes exist beyond the 15-GHz span. Figures 4(c) and 4(d) are zoom-in pictures around the beat note, with a span of 500 MHz (inset, 10 MHz) and 200 kHz, respectively. The strong oscillating envelope in Fig. 4(d) indicates high coherence of the locked fiber laser, which is far beyond the coherent length of the 13244-m fiber [20].

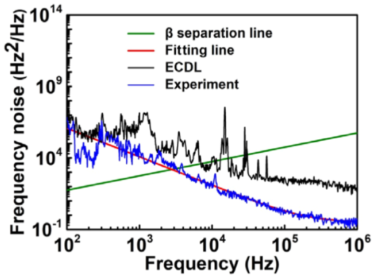

Fig. 5. Frequency noise spectra. Blue curve: frequency noise spectra of the locked fiber laser. Black curve: frequency noise spectra of a commercial ECDL for reference.

Differential phase noise of the locked fiber laser is measured at a frequency carrier of 40 MHz, using the DSHI with 48-m fiber delay [20]. Figure 5 shows single-sided frequency noise spectra of the locked laser (blue curve) transformed from the differential phase noise measurement, and frequency noise spectra of a commercial external cavity diode laser (ECDL, TOPTICA CTL 1550 nm, black curve) for reference. A noise model $S_\upsilon(f)$ composed of white frequency noise, flicker frequency noise, and random walk frequency noise is used to fit the measured noise spectra of the locked fiber laser [20], with best agreement shown in the red curve, where $S_\upsilon(f) = 0.3 + 5\times10^4/f + 1.2\times10^{10}/f^2$. Here, f is the Fourier frequency. The locked laser has a white frequency noise limit at $S_0 = 0.3\ \mathrm{Hz^2/Hz}$. Calculated from $\Delta\upsilon = S_0\pi$ [20], this corresponds to a fundamental linewidth of ~0.94 Hz. In the white frequency region, the frequency noise of the locked fiber laser is more than 23-dB lower than the ECDL laser. The β separation line is given by $S(f) = 8\times\ln 2\times f/\pi^2$, shown in the olive curve [21]. Noise spikes around 1 kHz of the frequency region come from the circumstances, which may be improved by better acoustical shielding of the laser system.

Single polarization of the locked fiber laser is measured by directing the output to the FPC-PBS setup, as shown in Fig. 2(5). PER is achieved by adjusting the FPC to make minimum and maximum powers at the S-port of the PBS. Minimum power measured at the S-port of the PBS (black curve) and PER calculated correspondingly (blue curve) are shown in Fig. 6. The high PER of ~40 dB reached is led by the injection-locking scheme for efficient single-longitudinal-mode selections, with other eigenmodes of the fiber laser suppressed. Maintaining of single-longitudinal-mode operation and its change to another orthogonal polarization working of the locked laser are also observed, by slightly tuning down the pumping current of 5.5 mA (from 687.2 mA to 681.7 mA), with the orthogonally polarized eigenmode on resonance of fiber-R. This tuning shows an on–off character at the P/S-port of the PBS.

In summary, we demonstrate an all-fiber narrow-linewidth single-polarization fiber laser realized on longitudinal mode selection and linewidth reduction from an external high finesse fiber-R. Single frequency lasing, high PER of ~40 dB, and very low white frequency noise at $0.3\ \mathrm{Hz^2/Hz}$ are measured, corresponding to a fundamental linewidth of ~0.94 Hz. With all non-polarization elements spliced together, we proves the realization of narrow-linewidth single-polarization fiber lasers in a simple and cost-effective way by making use of the external longitudinal mode selection and linear polarization of each eigenmode in the birefringent fiber laser. Better stability of

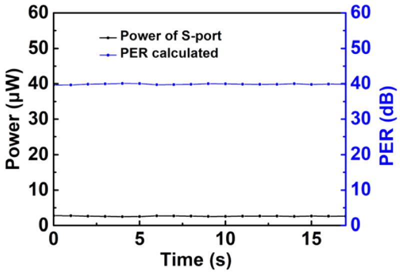

Fig. 6. Single polarization of the locked fiber laser. Black curve: minimum power measured at S-port of the PBS. Blue curve: PER calculated correspondingly.

the locked fiber laser can be expected with the special design of its thermal cooling system and packaging the laser with acoustical shields. Additionally, the long laser cavity can be further extended with double cladding fibers, combiners, and multi-mode pumpers to reach even higher laser power.

Funding. National Key Research and Development Program of China (2017YFA0303700, 2019YFA0705000); National Natural Science Foundation of China (11621091, 11627810, 11674169, 11690031, 51890861, 91950206); Leading-Edge Technology Program of Natural Science Foundation of Jiangsu Province (BK20192001); Key R&D Program of Guangdong Province (2018B030329001); Excellent Research Program of Nanjing University (ZYJH002).

Disclosures. The authors declare no conflicts of interest.

Data Availability. Data underlying the results presented in this Letter are not publicly available at this time but may be obtained from the authors upon reasonable request.

REFERENCES

1. K. Numata, J. Camp, M. A. Krainak, and L. Stolpner, Opt. Express **18**, 22781 (2010).
2. E. Rønnekleiv, Opt. Fiber Technol. **7**, 206 (2001).
3. J. Cariou, B. Augere, and M. Valla, C. R. Phys. **7**, 213 (2006).
4. D. G. Matei, T. Legero, S. Häfner, C. Grebing, R. Weyrich, W. Zhang, L. Sonderhouse, J. M. Robinson, J. Ye, F. Riehle, and U. Sterr, Phys. Rev. Lett. **118**, 263202 (2017).
5. C. W. Chou, D. B. Hume, T. Rosenband, and D. J. Wineland, Science **329**, 1630 (2010).
6. J. K. Perin, A. Shastri, and J. M. Kahn, J. Lightwave Technol. **35**, 4650 (2017).
7. S. L. I. Olsson, J. Cho, S. Chandrasekhar, X. Chen, P. J. Winzer, and S. Makovejs, Opt. Express **26**, 4522 (2018).
8. A. S. G. Andrae, ResearchGate, 2017, https://www.researchgate.net/publication/320225452_Total_Consumer_Power_Consumption_Forecast.
9. M. C. Collodo, F. Sedlmeir, B. Sprenger, S. Svitlov, L. J. Wang, and H. G. L. Schwefel, Opt. Express **22**, 19277 (2014).
10. B. Sprenger, H. G. L. Schwelfel, and L. J. Wang, Opt. Lett. **34**, 3370 (2009).
11. S. H. Xu, Z. M. Yang, T. Liu, W. N. Zhang, Z. M. Feng, Q. Y. Zhang, and Z. H. Jiang, Opt. Express **18**, 1249 (2010).
12. X. Huang, Q. Zhao, W. Lin, C. Li, C. Yang, S. Mo, Z. Feng, H. Deng, Z. Yang, and S. Xu, Opt. Express **24**, 18907 (2016).
13. L. Li, Y. Cao, Y. Zhi, J. Zhang, Y. Zou, X. Feng, B. Guan, and J. Yao, Light Sci. Appl. **9**, 169 (2020).
14. C. Li, S. Xu, X. Huang, Y. Xiao, Z. Feng, C. Yang, K. Zhou, W. Lin, J. Gan, and Z. Yang, Opt. Lett. **40**, 1964 (2015).
15. P. Laurent, A. Clairon, and C. Breant, IEEE J. Quantum Electron. **25**, 1131 (1989).
16. B. Dahmani, L. Hollberg, and R. Drullinger, Opt. Lett. **12**, 876 (1987).
17. H. Lee, M. Suh, T. Chen, J. Li, S. A. Diddams, and K. J. Vahala, Nat. Commun. **4**, 2468 (2013).
18. H. Lee, T. Chen, J. Li, K. Y. Yang, S. Jeon, O. Painter, and K. J. Vahala, Nat. Photonics **6**, 369 (2012).
19. A. L. Floch, G. Ropars, J. M. Lenormand, and R. L. Naour, Phys. Rev. Lett. **52**, 918 (1984).
20. W. Ma, B. Xiong, C. Sun, X. Ke, Z. Hao, L. Wang, L. Wang, J. Wang, Y. Han, H. Li, and Y. Luo, Appl. Opt. **58**, 3555 (2019).
21. G. D. Domenico, S. Schilt, and P. Thomann, Appl. Opt. **49**, 4801 (2010).